Carbon Nanostructures in Portable Fuel Cells: Single-Walled Carbon Nanotube Electrodes for Methanol Oxidation and Oxygen Reduction

G. Girishkumar,[†] K. Vinodgopal,*[,†,‡] and Prashant V. Kamat*[,†]

Radiation Laboratory and Department of Chemical and Biomolecular Engineering, University of Notre Dame, Notre Dame, Indiana 46556-0579, and Department of Chemistry, Indiana University Northwest, Gary, Indiana 46408

Received: July 14, 2004; In Final Form: September 24, 2004

We show here, for the first time, a reproducible way to obtain films of varying amounts of single-walled carbon nanotubes (SWCNTs) on electrode surfaces using electrophoretic deposition. We deposit these nanotubes in a facile manner on an optically transparent electrode (OTE) and investigate its performance as an electrode material in the presence of platinum for methanol oxidation and oxygen reduction. Our focus here is on the deposition of the SWCNT on the electrodes, the characterization of the nanotubes on the electrode surface, and the cyclic voltammetry of methanol oxidation and oxygen reduction using these nanostructured carbon electrodes with platinum electrodeposited on them. The nanotubes retain their structure on the electrode surface, and we can obtain electrodes with relatively thick films of the CNTs. The high surface area and porosity of these films enable us to use relatively small amounts of platinum and yet obtain excellent currents. We see a remarkable enhancement in methanol oxidation current relative to unsupported platinum. Analysis of the electrode kinetics using Tafel plots suggests that the CNT support provides a strong electrocatalytic effect in both reactions arising from their unique electrical properties.

Introduction

The operating principle for direct methanol fuel cells (DMFCs) involves the oxidation of methanol and the reduction of oxygen over precious metal catalysts such as platinum and ruthenium mixtures dispersed over a carbon support.[1−3] Consequently, the biggest barrier to widespread commercial use of these cells is the cost of the precious metals, and the need exists, therefore, to reduce the amount of such catalyst.[4,5] Such a reduction in the amount of metal catalyst can in most cases be achieved by increasing the amount of metal that is actually utilized on an electrode surface. One way to achieve this goal is by using high-surface-area carbon supports, which generally enables higher utilization of the metal catalyst.[6,7] Carbon nanostructures such as single-walled carbon nanotubes (SWCNTs) and fullerenes present themselves as potentially useful candidates for such applications.[8,9] In a recent communication, we showed that nanostructured carbon electrodes derived from fullerenes can serve as excellent supports for the platinum-catalyzed electro-oxidation of methanol.[10] Several recent works have also highlighted the use of carbon nanostructures as high-surface-area carbon supports for developing new electrode materials for DMFCs.[11−13] Lukehart et al have developed a graphite nanofiber composite with platinum which shows an enhanced methanol oxidation current relative to an unsupported catalyst.[14,15]

The unique electrical and structural properties of carbon nanotubes (CNT) have made them very attractive candidates for fuel cell applications.[16−18] CNTs can be classified as metallic or semiconducting according to their different electronic structures.[19] However, the synthesis, metal loading, and deposition of these nanotubes to produce a working electrode for useful applications remains a nontrivial task.[20] While some groups have used chemical vapor deposition and others have used a conventional ink process to make membrane electrode assemblies, the challenges in designing reproducible working electrodes for fuel cell applications using SWCNTs are still significant. In the case of the ink process, it is estimated that only 20−30% of the platinum catalyst is used because of the difficulty of accessing inner electrocatalytic sites.[21] Achieving a high degree of dispersion of platinum or other metal catalysts on the CNT support is an important goal, so as to make full avail of the latter's high surface areas, conductivity, and porosity.

We have developed a one-step solubilization procedure of carbon nanotubes in an organic solvent using a quaternary ammonium salt as the capping agent. In an earlier paper, we showed the ability to create self-assembled linear bundles of CNTs and align them under the influence of a dc electric field.[22] This in itself represents a substantial advancement in the ability to align the carbon nanotubes for practical applications. By varying the dc voltage in this electrophoretic procedure, we can deposit CNT films on electrode surfaces such as optically transparent electrodes. We have employed Raman spectroscopy and other imaging methods to show that the nanotubes' structures are retained on the electrode surface. A pulse plating method employed for the deposition of platinum nanocrystallites provides an efficient way to construct the CNT electrodes for applications such as DMFCs.[23,24] We have used these platinum-coated CNT electrodes in half-cell reactions to evaluate their performance in methanol oxidation and oxygen reduction reactions (ORR). The CNT electrodes show superior performance for methanol oxidation as compared to fullerene nanostructures. Similar enhancements are also seen in the cathode reaction.

* To whom correspondence should be addressed. E-mail: pkamat@nd.edu (P.K.), kvinod@iun.edu (K.V).
[†] University of Notre Dame.
[‡] Indiana University Northwest.

10.1021/jp046872v CCC: $27.50
Published on Web 12/08/2004

SCHEME 1: Schematic Representation of the Sequence of Events that Happens during the Solubilization and Electrophoretic Deposition of SWCNTs on an OTE

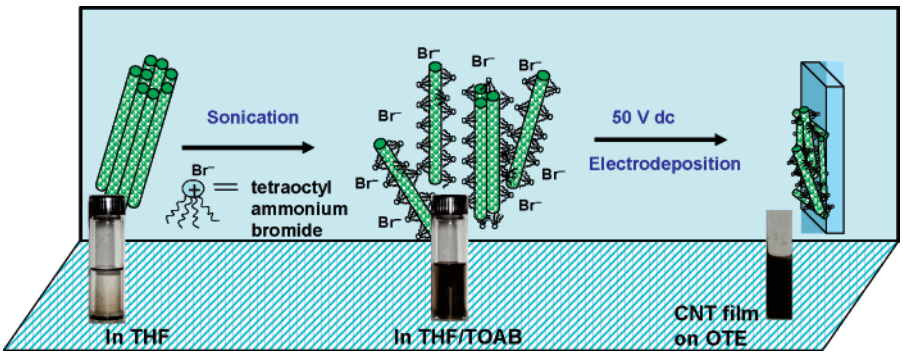

While CNT electrodes with platinum deposited on them have been used in earlier studies for both redox reactions, not much attention has been focused on the potential catalytic role of the nanotubes in the electrode reactions.[25] The answer to this question has important implications in improving the performance of an actual DMFC employing such an electrode configuration. The electrocatalytic effect of a CNT support in both the oxidation and reduction reactions should manifest itself in lower activation energies and better electron-transfer kinetics at the electrode interface. We have constructed Tafel plots and thereby obtained kinetic parameters for the electrode reactions on a SWCNT/Pt. Comparison with an unsupported platinum electrode provides powerful evidence of the electrocatalytic nature of the CNT support

Experimental Section

Solubilization of Carbon Nanotubes. SWCNTs were obtained from SES Research and used as is for the present study. Solubilization of the nanotubes was achieved by the following procedure: 10 mg of SWCNT was weighed and mixed with 0.13 g of tetraoctylammonium bromide (TOAB) in a centrifuge tube. To this, 25 mL of tetrahydrofuran (THF) was added and sonicated for 30 min to get a black suspension. It is evident that the presence of quaternary ammonium salt plays an important role by binding to SWCNT and enabling the latter to be suspended in polar solvents. The TOAB-coated CNTs prior to sonication are agglomerated and settle down. During sonication, the CNTs are exfoliated, which is evident from the dispersed CNTs in the solution. The TOAB binds to the surface of the CNT by hydrophobic interactions, thereby preventing aggregation and settling.[26,27]

The black suspension was centrifuged at 10 000 rpm for approximately 10 min. The clear supernatant liquid containing unbound TOAB was discarded. This procedure was repeated, and the final centrifugate, after removing the solvent, was dried. The repeated washing and centrifuging procedure allowed us to discard any unbound TOAB from the SWCNT material. The dried material consisting of TOAB-bound SWCNTs can be readily suspended in organic solvents. In the present experiments, TOAB-bound SWCNTs were resuspended in 25 mL THF by sonication for 10−15 min.

Electrophoretic Deposition of SWCNTs as Films on Electrode Surfaces. The optically transparent electrodes (OTEs) cut from a conducting glass plate (Pilkington) were pretreated by immersing in a 3% aqueous solution of aminopropoxysilane (APS) for 2 h. They were then rinsed in deionized water and allowed to dry in air under ambient conditions. A more uniform film of the CNT can be electrophoretically deposited on these APS pretreated electrodes. A 1.4-mL quantity of the CNT/TOAB suspension in THF was transferred to a 1-cm path length cuvette. Two APS-coated OTEs were kept at a distance of ~6 mm in the cuvette, using a Teflon spacer. Direct-current voltage was applied between the two electrodes using a Fluka 415 dc power supply. The deposition was done in different stages: 500 V was applied initially for 1 min, resulting in a thin deposit of the CNT on OTE. As reported earlier, we observe aligned bundles at this high dc voltage.[22] The solution was then sonicated again for 1 min, and the electrodeposition was continued by maintaining at 50 V for 2 min. The solution turns completely colorless, and the entire TOAB-coated CNT can thus be deposited on the OTE. The solubilization and deposition sequence is illustrated in Scheme 1.

To estimate the amount of SWCNTs, we have weighed the electrodes individually before and after electrodeposition. Thus, the maximum amount of SWCNT on the OTE was found to be 6 mg. The contribution from TOAB is expected to be in the range of 5−10 wt %. The electrode was then dried in air and stored in desiccators for further experimental use.

The CNT on the OTE was characterized by Raman and microscopic imaging methods. The Raman measurements were made on a Jasco RMP-210 Raman spectrometer. The laser power used was 10 mW. A radiation spot of 0.1-mm diameter was used in 180° backscattering geometry at room temperature. The excitation wavelength was 514 nm. Atomic Force Microscope (AFM) images of the nanotubes on an OTE surface (1 cm × 1 cm size) were obtained using a digital Nanoscope IIIa atomic force microscope. Characterization of the surface was carried out in the tapping mode with silicon tips (Nanoprobe tapping mode TAP 300, TESP). Transmission electron microscope (TEM) images of CNT were obtained at high resolution on a Hitachi H600 transmission electron microscope. To obtain the TEM images, a single drop of a dilute suspension of the TOAB-bound CNT in THF was deposited on 3-mm Cu grids. The TEM images of the CNTs with platinum particles deposited on them were obtained by sonicating the CNT/OTE in THF solution. A drop of the resulting suspension in THF was then used to obtain the TEM image.

Platinum nanoparticles were electrodeposited on the OTE/SWCNT films by electrochemical reduction of $PtCl_6^{2-}$. A 1.4 cm^2 area of the SWCNT film on the OTE was immersed in an aqueous solution of hexachloroplatinic acid, and reduction was carried out by applying a sequence of pulses (pulses of 12 ms duration) with a duty factor of 0.5 at a potential of −350 mV versus saturated calomel electrode (SCE). All electrochemical studies were carried out using a BAS 100 electrochemical analyzer. A three-electrode cell consisting of the SWCNT electrode as the working electrode, platinum as counter electrode, and SCE as reference electrode was used in all cases. It

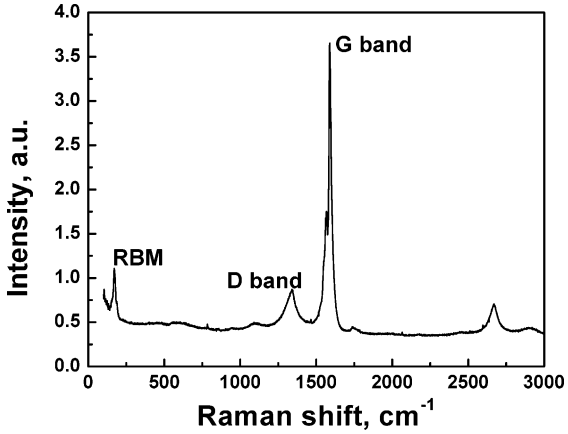

Figure 1. Raman spectra of a TOAB-coated SWCNT electrodeposited on an optically transparent electrode. The spectrum shown is an average of two acquisitions and the TOAB-CNT loading on the sample is estimated to be less than 1 mg.

is known that platinum deposition begins at a potential of 200 mV versus SCE, and a significant current is observed at negative potentials. Hence, we have used −350 mV versus SCE as the deposition potential.[28] The amount of platinum deposited in each case can be determined by chronocoulometry. This has been done by electronic integration of the current versus time curve for each pulse such that the total charge amounts to 0.1 C. From Faraday's law, we calculate a loading of 56 μg/cm^2 of the Pt corresponding to a charge of 0.1 C.

Results and Discussion

Characterization of Carbon Nanotubes. Raman spectroscopy has been used as a tool in the present case to identify signatures that are pertinent to SWCNT electrodeposited on an OTE. A Raman spectrum of the CNTs electrodeposited on OTEs is shown in Figure 1. The spectral features indicate that CNT retains its intact structure during the process of electrodeposition. While the TOAB surfactant helps to separate the nanotubes, they are also expected to have some effect on the Raman spectrum. The ring breathing mode (RBM) and the D and G lines are characteristic signatures of single-walled nanotubes.[29,30] The RBM in particular has been used to determine the internal diameter of the nanotubes.[31] The frequency, ω_{rbm}, of this mode depends on the tube diameter d according to the relation

$$\omega_{rbm} = \alpha/d_i + B \qquad (1)$$

where $\alpha = 232 \pm 10$ cm^{-1} and $B = 10$ cm^{-1}.[31] Our initial results give us nanotube diameters close to 1.4 nm.[32,33] The tangential G-band modes can also provide information about the metallic versus the semiconducting nature of the nanotubes on the electrode surface.[34] The profile of the G band that we observe in our case suggests a semiconducting nature, although subsequent metal deposition could significantly affect the mode and the characteristic properties of the CNTs. Thus, we obtain direct evidence that the CNT nanostructure is retained on the electrode surface after electrodeposition.[35]

Additional confirmation that the nanotubes retain their structure is available from the tapping mode AFM image of the SWCNT/OTE shown in Figure 2. The corresponding TEM image (Figure 3A) of the nanotubes is shown in Figure 3A. Both the AFM and TEM images show the presence of interconnected bundles, isolated strands, as well as loops of varying diameters. The catalyst particles associated with the synthesis of these tubes are seen in the TEM image as dark

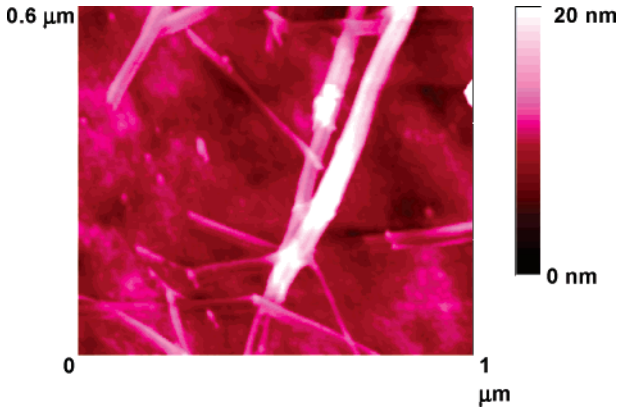

Figure 2. Tapping-mode AFM image of SWCNT deposited by electrophoresis on an OTE surface. The CNT loading on the sample is estimated to be less than 1 mg.

spots at the nodes where the different bundles interconnect. The other spots on the surface of the tubes are most likely TOAB surfactant molecules arising from our solubilization procedure.

We have also characterized the nanotubes following deposition of platinum on them. Platinum was deposited on the nanotubes by pulsed electrochemical deposition at −350 mV from a solution of $PtCl_6^{2-}$. It is known that pulsing can give rise to uniform particle size and a good distribution. By varying the duration of the pulse, we can get particles of varying diameters (not shown). After the Pt deposition, the electrodes were sonicated in THF solution. A drop of the resulting suspension in THF was then used to obtain a TEM image. Figure 3B shows the TEM image of SWCNT at a lower magnification after the deposition of platinum clusters. The dark spots seen in Figure 3B are platinum crystallites of 20 nm size. The striking feature of this image is that the platinum particles are attached exclusively to the nanotubes, thereby ensuring a close interaction with the CNT support.

Oxidation of Methanol using Platinum-Deposited SWNT Electrodes (OTE/CNT/Pt). The larger surface area of the nanotubes and the close contact between the platinum catalyst and the carbon surface as seen in the AFM and TEM images should make the OTE/CNT/Pt system ideal for methanol oxidation. The electrochemical activity of such a system has been tested in a cyclic voltammetry experiment by oxidizing 1.8 M methanol in 1 M H_2SO_4 solution as shown in Figure 4. Methanol oxidation is represented by the anodic peak around 800 mV. In the reverse scan, the adsorbed intermediates produce a second oxidation peak at ~650 mV. The magnitude of the peak current at 800 mV is directly proportional to the amount of methanol oxidized at the electrode.

We observe methanol oxidation currents between 50 and 60 mA/cm^2 at an OTE/CNT/Pt electrode. In the absence of nanotubes, oxidation of methanol on an OTE with an equal amount of platinum yields typically about 6 mA/cm^2 of current. The enhancement in the oxidation current observed with nanotubes is indicative of the important role they play in promoting the methanol oxidation. The cyclic voltammetry studies show an initial activation period as the oxidation current increases with repetitive scans between 0 and 1.0 V. The oxidation current eventually reaches a plateau after about the sixth cycle. These cycles can be reproduced without noticing any deterioration in the magnitude of current values.

To optimize the amount of CNT for methanol oxidation, we have prepared several electrodes and studied the effect of loading of CNT on methanol oxidation as indicated in Figure 5A. The amount of solubilized CNT deposited on the OTE was deter-

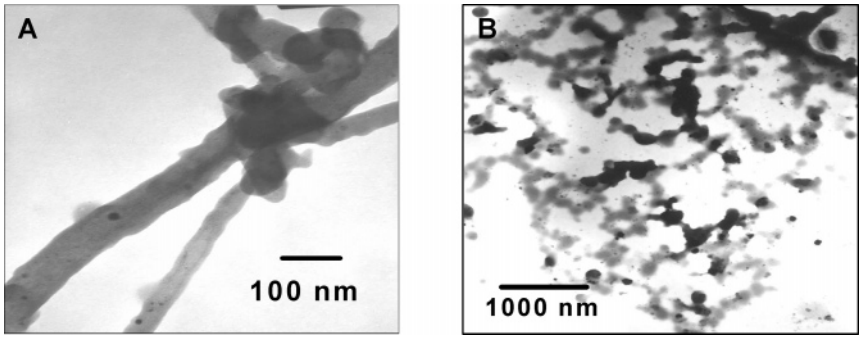

Figure 3. (A) Transmission electron micrograph image of TOAB bound CNT clusters. (B) TEM image of SWCNT clusters with platinum crystallites electrodeposited on them.

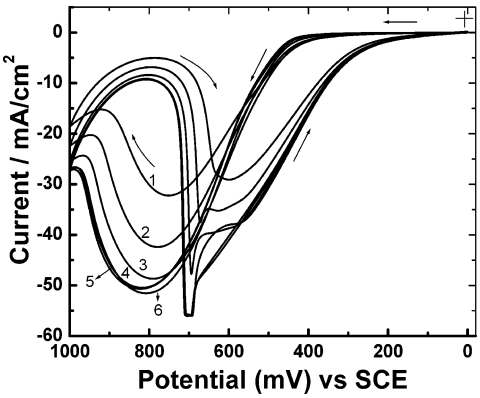

Figure 4. Cyclic voltammetric traces of methanol oxidation (1.8 M) in 1 M H_2SO_4 recorded using OTE/CNT/Pt system. Traces 1−6 correspond to successive scans showing the stabilization of the oxidation current peak. Scan rate was 20 mV/s. Platinum loading was 0.14 mg/cm^2 and the amount of TOAB-CNT is ∼6 mg/cm^2.

mined by weighing the OTE before and after CNT deposition. As we increase the loading of CNT, the magnitude of the current value increases, suggesting a catalytic role for the CNT. In all these cases, we have maintained the same amount of platinum loading.

In a similar set of experiments, the loading of platinum on the CNT can be optimized by increasing the amount of platinum that has been deposited while keeping the amount of carbon nanotubes constant. Figure 5B shows the current for the oxidation of methanol at an OTE/CNT/Pt electrode as a function of platinum coverage. The highest oxidation currents are obtained at a platinum loading of 0.14 mg/cm^2. To ascertain the effect of the carbon nanotubes in enhancing the oxidation current, we have also carried out a similar experiment without CNT (viz., Pt on a bare OTE). The oxidation currents observed with varying amounts of platinum on a bare OTE are also shown in Figure 5B. Comparison of the two curves in Figure 5B shows significantly higher oxidation currents for CNT-supported catalyst. While it is unlikely that we have identical surface areas for the same platinum loading on both bare OTE and CNT film, it is clear that there is a substantial increase in the oxidation current in the presence of CNT.

While we cannot rule out the contribution from varying surface areas for similar platinum loadings, the trend of higher current observed with increased Pt loading on CNT electrodes indicates the beneficial role of the nanotubes. To resolve this issue, we have examined the kinetic aspects of methanol oxidation on a CNT/Pt electrode.

Kinetics of Methanol Oxidation Reaction on CNT/Pt Electrode. Understanding the kinetics of methanol oxidation on SWCNT and comparing the results with pure platinum is

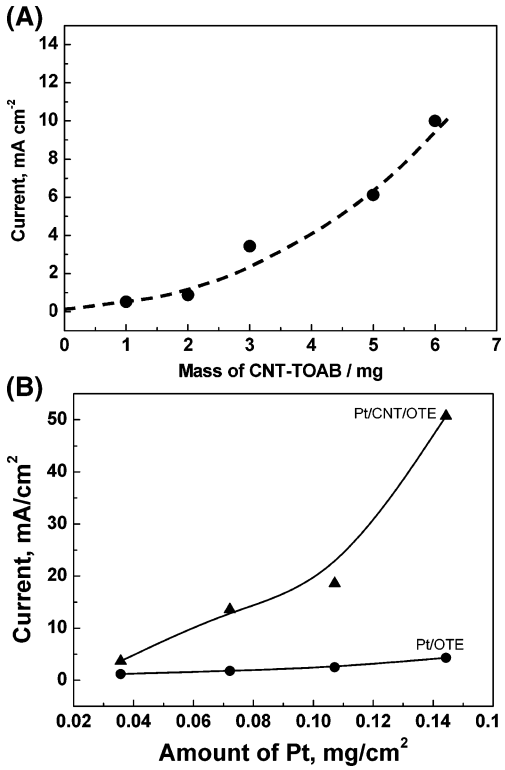

Figure 5. (A) Dependence of the methanol oxidation current on the mass loading of the CNT. Platinum loading was 0.07 mg/cm^2. (B) Dependence of the methanol oxidation current on the loading of Pt in an OTE/CNT/Pt system. The electrolyte in both cases was 1.8 M methanol in 1 M H_2SO_4. The TOAB-CNT loading is ∼6 mg/cm^2. Also shown is the dependence of the methanol oxidation current on the loading of Pt in a bare Pt/OTE system.

necessary to prove the electrocatalytic activity of CNT toward methanol oxidation. A blank OTE with the same amount of Pt deposition was used for comparison. Tafel plots (Figure 6) were obtained from the onset region of the linear polarization curve at higher overpotentials from the reduced form of the Butler−Volmer equation[36]

$$\log i = \log i_0 + \frac{\alpha_A nF}{2.303RT}\eta \qquad (2)$$

where η is the overpotential, i_0 is the exchange current density, and α is the anodic transfer coefficient, and all other symbols have their usual meanings. The linear polarization curves are obtained from the linear scan voltammogram (LSV) shown in the inset of Figure 6. These voltammograms reveal that the SWCNT/Pt electrode is more active than unsupported platinum. The onset potential for the methanol oxidation is at a much

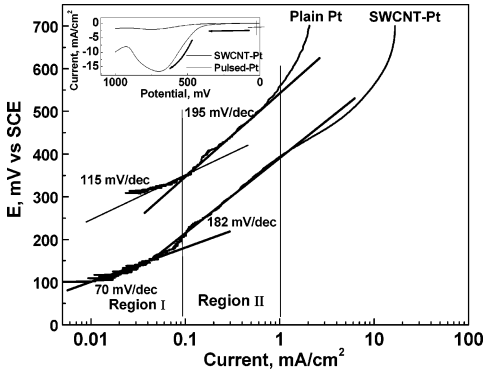

Figure 6. Comparison of the Tafel plot for the methanol oxidation on a pulsed Pt electrode and an electrode modified with SWCNT and Pt. The loading of Pt in both cases was the same (0.1 mg/cm^2). The inset indicates the typical linear sweep voltammogram (LSV) for a SWCNT-modified Pt electrode and an unsupported Pt electrode (scan rate: 20 mV/s

lower potential for the CNT/Pt electrode (200 mV vs SCE) than the unsupported Pt electrode (400 mV). This reduction of the onset potential for the methanol oxidation reaction on a CNT/Pt electrode is comparable to the effect observed with a mixture of ruthenium on platinum.[37,38]

The effect of ruthenium and the mechanism by which it inhibits CO poisoning of the Pt surface is now well-established.[39,40] Ru−OH species are formed on the catalyst surface according to the following equation:

$$\mathrm{Ru} + \mathrm{H_2O} \rightarrow \mathrm{RuOH} + \mathrm{H^+} + \mathrm{e^-} \qquad (3)$$

These RuOH species react with CO linearly bonded to Pt, which is the final intermediate of methanol oxidation on Pt.[41]

$$\mathrm{RuOH} + \mathrm{PtCO} \rightarrow \mathrm{Pt{-}Ru} + \mathrm{H^+} + \mathrm{CO_2} + \mathrm{e^-} \qquad (4)$$

The reaction of the ruthenium with adsorbed water (reaction 3) occurs at lower anodic potentials. This shift in the onset potential has been attributed to the reduced work function of Ru as compared to Pt. (Φ_{Pt} = 5.36 eV; Φ_{Ru} = 4.52 eV). The comparable shift in anodic potential that we observe with CNT supports can also be attributed to a similar change in the work function for CNTs ($\Phi_{CNT} \approx 5$ eV).[42,43] A consequence of the reduced CNT work function is the spontaneous reduction of metal ions on carbon nanotubes recently reported by Dai et al.[44] We conclude that the potential shift along with the enhancement of the anodic current using CNT electrodes arises from a catalytic role for CNT in promoting the methanol oxidation process.

Two distinct slopes are evident from our Tafel plots in Figure 6. In region I, where the currents are low, we obtain a slope of 115 mV/decade for the Pt electrode and a slope of 70 mV/decade for the CNT/Pt electrode. In region II, where there is a rapid increase in the slope, we obtain values of 195 and 182 mV/decade for the Pt and CNT/Pt electrodes, respectively. The variations observed in region I suggest that different electrode kinetics is operative for methanol oxidation at the CNT/Pt electrode. Values of 110−140 mV/decade have been reported for carbon-supported Pt−Ru catalysts, while a much lower value of 60 mV/decade has been reported for ruthenium deposited on a Pt single-crystal electrode.[45,46] The shift in the onset potential for methanol oxidation and the reduced activation energies obtained from the Tafel slope suggest that the CNTs have a major catalytic effect on the surface reactions that occur during the oxidation of methanol. Britto et al. have shown

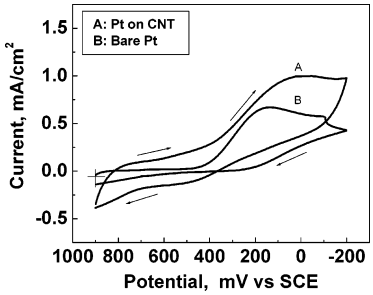

Figure 7. Cyclic voltammetric traces in a 0.5 M H_2SO_4 saturated with oxygen: A. SWCNT/Pt electrode (4.3 mg/cm^2 SWCNT and 0.04 mg/cm^2 Pt). B. Unsupported Pt (0.04 mg/cm^2). Scan rate is 20 mV/s.

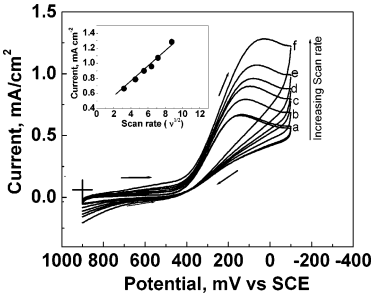

Figure 8. Cyclic voltammetric traces at an OTE/CNT/Pt electrode (4.3 mg/cm^2 SWCNT and 0.04 mg/cm^2 Pt) for the oxygen reduction reaction at various scan rates. The electrolyte was 0.5 M H_2SO_4 saturated with oxygen. The inset in the figure indicates the dependence of peak current on scan rate.

improved charge transfer at carbon nanotube electrodes.[47] All of the evidence points to a similar effect in the case of methanol oxidation on CNTs.

Electrocatalytic Activity of O_2 Reduction. The oxygen reduction reaction (ORR) and its kinetic limitations are of fundamental interest from the viewpoint of fuel cell applications. A careful study of the literature indicates that platinum particles on a variety of carbon supports are still the most efficient catalyst for the cathode in a fuel cell. One of the major problems with the bare carbon support is the sluggish kinetics of the ORR. The sluggish kinetics of the ORR leads to a loss in cell voltage of 400 mV under typical fuel cell operating conditions. In our present effort, we focus our attention on a SWCNT/Pt electrode and its performance as a cathode catalyst for the ORR.

For the oxygen reduction experiments at the SWCNT/Pt electrodes, a solution of 0.1 M H_2SO_4 was purged with ultrapure oxygen for ∼15 min, so that the solution becomes completely saturated with oxygen.[17] The electrode was repetitively scanned over a potential range from 1000 to −200 mV several times to ensure reproducibility. Figure 7 indicates the cyclic voltammograms for the ORR on a SWCNT electrode electrodeposited with Pt (Figure 7A), and unsupported Pt (Figure 7B).

The oxygen reduction process proceeds by two different reaction pathways in acidic medium: the direct four-electron pathway (Equation 5) and the peroxide pathway (Equation 6).[48,49]

$$\mathrm{O_2} + 4\mathrm{H^+} + 4\mathrm{e^-} \rightarrow 4\mathrm{OH^-}\ (E^0 = 1.23\ \mathrm{V\ vs\ SHE}) \qquad (5)$$

$$\mathrm{O_2} + 2\mathrm{H^+} + 2\mathrm{e^-} \rightarrow \mathrm{H_2O_2}\ (E^0 = 0.67\ \mathrm{V\ vs\ SHE}) \qquad (6)$$

It should be noted that the cathodic current is a sum of the oxygen reduction current and the double-layer charging effects, but the enhancement in the reduction current is clearly distinguishable. The anchoring of the Pt catalyst on the carbon

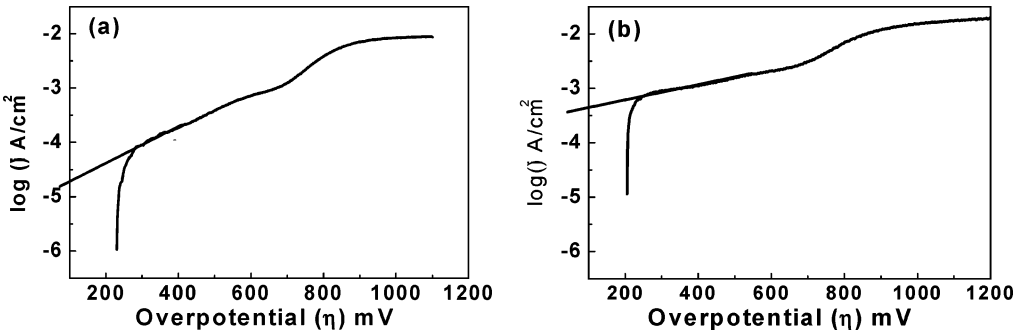

Figure 9. Tafel polarization curve for bare Pt (a) and SWCNT-modified Pt (b). The plot was obtained from the voltammogram for the O_2 reduction reaction.

nanotube surface has a pronounced effect on the cathodic current. It can be seen from the cyclic voltammogram in Figure 7 that the current values for the ORR on SWCNT-based electrodes are higher by a factor of 1.5 relative to unsupported platinum particles. The loading of the Pt catalyst was kept constant in both of these cases. Paulus et al. have reported a similar enhancement in current values using Pt−Co, Pt−Cr, and Pt−Ni alloys.[50] Figure 8 shows the cyclic voltammograms of the OTE/SWCNT/Pt electrode at different scan rates. The peak current increases linearly with the square root of the scan rate as shown in the inset of Figure 8. This indicates that the diffusion of oxygen to the electrode surfaces is the current-limiting process. Good reproducibility of the oxygen reduction behavior was tested by repeating the experiments using several different electrodes.

Tafel plots were obtained from the onset region of the linear polarization curve at higher overpotentials from the reduced form of the Butler−Volmer equation given earlier (equation 2). A plot of log i versus overpotential (η) for the unsupported platinum on OTE and OTE/SWCNT/Pt is shown in Figure 9. The Tafel slope obtained from this plot is −59 mV/decade for the unsupported Pt electrode and −38 mV/decade for the SWCNT/Pt. We have not used any correction for any mass transfer effects, and the values vary depending upon the substrate.[51] The slope observed for the unsupported platinum is consistent with literature values.[52,53] The exchange current density is obtained by extrapolating the linear region to zero overpotential. We obtain an exchange current density value from this analysis of 6.3×10^{-4} A/cm^2 for OTE/SWCNT/Pt, which is an order of magnitude higher than the value of 1.9×10^{-5} A/cm^2 for the unsupported Pt/OTE. The former value compares very favorably with the value of 1.09×10^{-7} A/cm^2 reported for a commercial catalyst such as platinum black.[47] Because the exchange current density depends on the nature of the electrode, this suggests that the OTE/SWCNT/Pt is a better electrocatalyst to promote the oxygen reduction reactions.

Conclusions

Using a simple electrophoretic procedure, we have successfully deposited carbon nanotubes on electrode surfaces. These films are robust and provide new ways to explore the electrochemical and electrocatalytic properties of carbon nanotube films. Pt deposited on SWCNT film has been shown to possess a higher catalytic activity for methanol oxidation and oxygen reduction than unsupported Pt on an OTE surface. The higher catalytic activity has been attributed to larger surface area provided by the carbon nanotube architecture and decreased overvoltage for methanol oxidation and oxygen reduction. The results presented in this study highlight the use of carbon nanotubes as a potential candidate for the development of miniaturized fuel cells.

Acknowledgment. The research described herein was supported by the U.S. Army CECOM RDEC through Agreement DAAB07-03-3-K414. Such support does not constitute endorsement by the U.S. Army of the views expressed in this publication. This is contribution no. NDRL 4538 from Notre Dame Radiation Laboratory.

References and Notes

(1) Parsons, R.; Vandernoot, T. *J. Electroanal. Chem.* **1988**, *257*, 9.
(2) Wasmus, S.; Kuver, A. *J. Electroanal. Chem.* **1999**, *461*, 14.
(3) Arico, A. S.; Srinivasan, S.; Antonucci, V. *Fuel Cells* **2001**, *1*, 133.
(4) Dillon, R.; Srinivasan, S.; Arico, A. S.; Antonucci, V. *J. Power Sources* **2004**, *127*, 112.
(5) Arico, A. S.; Baglio, V.; Modica, E.; Di Blasi, A.; Antonucci, V. *Electrochem. Commun.* **2004**, *6*, 164.
(6) Hogarth, M. P.; Munk, J.; Shukla, A. K.; Hamnett, A. *J. Appl. Electrochem.* **1994**, *24*, 85.
(7) Gloaguen, F.; Leger, J. M.; Lamy, C. *J. Appl. Electrochem.* **1997**, *27*, 1052.
(8) Che, G. L.; Lakshmi, B. B.; Fisher, E. R.; Martin, C. R. *Nature* **1998**, *393*, 346.
(9) Che, G. L.; Lakshmi, B. B.; Martin, C. R.; Fisher, E. R. *Langmuir* **1999**, *15*, 750.
(10) Vinodgopal, K.; Haria, M.; Meisel, D.; Kamat, P. *Nano Lett.* **2004**, *4*, 415.
(11) Rajesh, B.; Thampi, K. R.; Bonard, J. M.; Mathieu, H. J.; Xanthopoulos, N.; Viswanathan, B. *Chem. Commun.* **2003**, 2022.
(12) Li, W. Z.; Liang, C. H.; Qiu, J. S.; Zhou, W. J.; Han, H. M.; Wei, Z. B.; Sun, G. Q.; Xin, Q. *Carbon* **2002**, *40*, 791.
(13) Serp, P.; Corrias, M.; Kalck, P. *Appl. Catal., A* **2003**, *253*, 337.
(14) Steigerwalt, E. S.; Deluga, G. A.; Lukehart, C. M. *J. Phys.Chem. B* **2002**, *106*, 760.
(15) Boxall, D. L.; Kenik, E. A.; Lukehart, C. M. *Chem. Mater.* **2002**, *14*, 1715.
(16) Liu, Z. L.; Lin, X. H.; Lee, J. Y.; Zhang, W.; Han, M.; Gan, L. M. *Langmuir* **2002**, *18*, 4054.
(17) Li, W. Z.; Liang, C. H.; Zhou, W. J.; Qiu, J. S.; Zhou, Z. H.; Sun, G. Q.; Xin, Q. *J. Phys. Chem. B* **2003**, *107*, 6292.
(18) Sun, X.; Li, R.; Villers, D.; Dodelet, J. P.; Desilets, S. *Chem. Phys. Lett.* **2003**, *379*, 99.
(19) Ouyang, M.; Huang, J.-L.; Lieber, C. M. *Acc. Chem. Res.* **2002**, *35*, 1018
(20) Barisci, J. N.; Wallace, G. G.; Baughman, R. H. *J. Electrochem. Soc.* **2000**, *147*, 4580.
(21) Wang, C.; Waje, M.; Wang, X.; Tang, J. M.; Haddon, R. C.; Yan, Y. S. *Nano Lett.* **2004**, *4*, 345.
(22) Kamat, P. V.; Thomas, K. G.; Barazzouk, S.; Girishkumar, G.; Vinodgopal, K.; Meisel, D. *J. Am. Chem. Soc.* **2004**, *126*, 10757.
(23) Kim, H.; Popov, B. N. *Electrochem. Solid State Lett.* **2004**, *7*, A71.
(24) Tang, H.; Chen, J. H.; Huang, Z. P.; Wang, D. Z.; Ren, Z. F.; Nie, L. H.; Kuang, Y. F.; Yao, S. Z. *Carbon* **2004**, *42*, 191.
(25) He, Z. B.; Chen, J. H.; Liu, D. Y.; Tang, H.; Deng, W.; Kuang, W. F. *Mater. Chem. Phys.* **2004**, *85*, 396.
(26) Niyogi, S.; Hamon, M. A.; Perea, D. E.; Kang, C. B.; Zhao, B.; Pal, S. K.; Wyant, A. E.; Itkis, M. E.; Haddon, R. C. *J. Phys. Chem. B* **2003**, *107*, 8799.
(27) Shvartzman-Cohen, R.; Levi-Kalisman, Y.; Nativ-Roth, E.; Yerushalmi-Rozen, R. *Langmuir* **2004**, *20*, 6085.
(28) Natter, H.; Hempelmann, R. *Electrochim. Acta* **2003**, *49*, 51.
(29) Heller, D. A.; Barone, P. W.; Swanson, J. P.; Mayrhofer, R. M.; Strano, M. S. *J. Phys. Chem. B* **2004**, *108*, 6905.
(30) Doorn, S. K.; Heller, D. A.; Barone, P. W.; Usrey, M. L.; Strano, M. S. *Appl. Phys. A* **2004**, *78*, 1147.

(31) Dresselhaus, M. S.; Dresselhaus, G.; Jorio, A.; Souza, A. G.; Pimenta, M. A.; Saito, R. *Acc. Chem. Res.* **2002**, *35*, 1070.

(32) Jorio, A.; Pimenta, M. A.; Souza, A. G.; Saito, R.; Dresselhaus, G.; Dresselhaus, M. S. *New J. Phys.* **2003**, *5*.

(33) Saito, R.; Gruneis, A.; Samsonidze, G. G.; Brar, V. W.; Dresselhaus, G.; Dresselhaus, M. S.; Jorio, A.; Cancado, L. G.; Fantini, C.; Pimenta, M. A.; Souza, A. G. *New J. Phys.* **2003**, *5*.

(34) Stoll, M.; Rafailov, P. M.; Frenzel, W.; Thomsen, C. *Chem. Phys. Lett.* **2003**, *375*, 625.

(35) Hulman, M.; Pfeiffer, R.; Kuzmany, H. *New J. Phys.* **2004**, *6*.

(36) Bard, A. J.; Faulkner, L. R. *Electrochemical methods. Fundamentals and Applications*, 2nd ed.; John Wiley & Sons: New York, 2001.

(37) Watanabe, M.; Motoo, S. *J. Electroanal. Chem.* **1975**, *60*, 267.

(38) Tremiliosi, G.; Kim, H.; Chrzanowski, W.; Wieckowski, A.; Grzybowska, B.; Kulesza, P. *J. Electroanal. Chem.* **1999**, *467*, 143.

(39) Maillard, F.; Gloaguen, F.; Leger, J. M. *J. Appl. Electrochem.* **2003**, *33*, 1.

(40) Long, J. W.; Stroud, R. M.; Swider-Lyons, K. E.; Rolison, D. R. *J. Phys. Chem. B* **2000**, *104*, 9772.

(41) Chrzanowski, W.; Wieckowski, A. *Langmuir* **1998**, *14*, 1967.

(42) Kazaoui, S.; Minami, N.; Matsuda, N.; Kataura, H.; Achiba, Y. *Appl. Phys. Lett.* **2001**, *78*, 3433.

(43) Suzuki, S.; Bower, C.; Watanabe, Y.; Zhou, O. *Appl. Phys. Lett.* **2000**, *76*, 4007.

(44) Choi, H. C.; Shim, M.; Bangsaruntip, S.; Dai, H. J. *J. Am. Chem. Soc.* **2002**, *124*, 9058.

(45) Gojkovic, S. L.; Vidakovic, T. R. *Electrochim. Acta* **2001**, *47*, 633.

(46) Gojkovic, S. L.; Vidakovic, T. R.; Durovic, D. R. *Electrochim. Acta* **2003**, *48*, 3607.

(47) Britto, P. J.; Santhanam, K. S. V.; Rubio, A.; Alonso, J. A.; Ajayan, P. M. *Adv. Mater.* **1999**, *11*, 154.

(48) Damjanovic, A.; Brusic, V. *Electrochim. Acta* **1967**, *12*, 615.

(49) Shukla, A. K.; Raman, R. K. *Annu. Rev. Mater. Res.* **2003**, *33*, 155.

(50) Paulus, U. A.; Wokaun, A.; Scherer, G. G.; Schmidt, T. J.; Stamenkovic, V.; Radmilovic, V.; Markovic, N. M.; Ross, P. N. *J. Phys. Chem. B* **2002**, *106*, 4181.

(51) Gojkovic, S. L.; Zecevic, S. K.; Savinell, R. F. *J. Electrochem. Soc.* **1998**, *145*, 3713.

(52) Wang, J.; Swain, G. M. *J. Electrochem. Soc.* **2003**, *150*, E24.

(53) Kita, H.; Gao, Y. Z.; Nakato, T.; Hattori, H. *J. Electroanal. Chem.* **1994**, *373*, 177.